ACS APPLIED MATERIALS & INTERFACES

RESEARCH ARTICLE

www.acsami.org

Work Function of Vanadium Dioxide Thin Films Across the Metal-Insulator Transition and the Role of Surface Nonstoichiometry

Changhyun Ko,* Zheng Yang, and Shriram Ramanathan

School of Engineering and Applied Sciences, Harvard University, Cambridge, Massachusetts 02138, United States

ABSTRACT: Vanadium dioxide (VO_2) undergoes a sharp metal-insulator transition (MIT) in the vicinity of room temperature and there is great interest in exploiting this effect in novel electronic and photonic devices. We have measured the work function of vanadium dioxide thin films across the phase transition using variable temperature Kelvin force microscopy (KFM). The work function is estimated to be ~5.15 eV in the insulating phase and increases by ~0.15 eV across the MIT. We further show that the work function change upon the phase transition is highly sensitive to near-surface stoichiometry studied by X-ray photoelectron spectroscopy. This change in work function is distinct from bulk resistance-versus temperature trends commonly used to evaluate synthesis protocols for such vanadium oxide films and optimize stoichiometry. The results are pertinent to understanding fundamental electronic properties of vanadium oxide as well as charge injection phenomena in solid-state devices incorporating complex oxides containing multivalence cations.

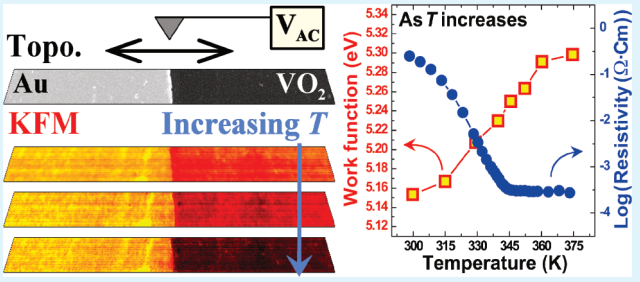

KEYWORDS: vanadium dioxide, thin film, metal-insulator transition, near-surface stoichiometry, Kelvin force microscopy, work function, X-ray photoelectron spectroscopy

1. INTRODUCTION

The mechanism governing metal-insulator transition (MIT) in vanadium dioxide (VO_2) is an intensively explored subject in condensed matter sciences.[1] Although electron−electron interactions leading up to the Mott interaction may cause the transition, structural transformation which occurs concurrently with MIT at ~340 K opens another possibility, Peierls instability.[2,3] The phase structure of VO_2 changes from rutile to monoclinic under cooling accompanied by cell size doubling and tilted V−V pair formation, possibly leading to band gap opening.[3] There is also a substantial technological interest in exploiting the ultrafast phase transition in advanced electronics and optoelectronics. It is to be noted, however, that the elementary electronic properties of VO_2 such as intrinsic carrier concentration, work function, and dielectric properties in thin film structures have not yet received much attention. The existence of multiple valence states of V complicates the material chemistry and in particular controlling surface stoichiometry is of importance.[4] Although it is rather well-known that vanadium oxides can be nonstoichiometric because of the ability of vanadium to exist in several valence states,[4] the work function and its dependence on near-surface stoichiometry is poorly understood. Surfaces may contact electrodes and hence affect barriers for charge injection, and in many devices, the near-surface regions may serve as channel layers and carrier concentration is of critical importance. Another example could be the use of phase transition layers as switchable ultrathin tunnel barriers, in which case the near-surface region would again be a crucial part of the whole structure.

The work function, Φ, defined as an amount of energy required to extract an electron from Fermi energy level of material surface to vacuum, is relevant to designing electronic devices such as metal-oxide junctions and field-effect devices.[5] Also, by measuring Φ across the transition boundary, the surface phase transition characteristics can be studied.[6] A few measurements of work function from VO_2 nanostructures have been reported previously.[7,8] Wang et al. measured the Φ of VO_2 nanorods of body-centered cubic structure as ~4.81 eV from ultraviolet photoelectron spectroscopy (UPS) at room temperature.[7] Recently, Yin et al. estimated the Φ of VO_2 nanobundles also using UPS and observed the decrease of Φ via MIT from ~4.10 eV in the insulating monoclinic phase to ~3.65 eV in the metallic rutile phase. In our study, Kelvin force microscopy (KFM) has been used to investigate Φ variation driven by MIT on the surface of VO_2 thin films. KFM is a scanning probe microscopy technique to measure contact potential difference (CPD) and topography simultaneously.[9−11]

In this manuscript, we report Φ values of vanadium dioxide film surface as a function of temperature spanning the phase transition. Also, two main observations from systematic temperature-variable KFM studies along with detailed conduction transport measurements and X-ray photoelectron spectroscopy (XPS) analysis: (1) Φ of VO_2 film surface increases slightly across phase boundary by heating and (2) the phase transition characteristics in the near-surface region of VO_2 films are clearly differentiated from those of VO_2 film bulk due to stoichiometry variation from surface to film interior. In addition, it was also

Received: May 17, 2011
Accepted: August 9, 2011
Published: August 09, 2011

observed that the degree of MIT-induced variation in both Φ and resistivity of VO_2 films are affected by oxygen stoichiometry.

2. EXPERIMENTAL DETAILS

2.1. VO_2 Synthesis. Highly textured vanadium oxide films were grown on single crystal Al_2O_3 (0001) by RF-sputtering from a VO_2 target (99.5%, AJA International Inc.). During synthesis, the substrate temperature and RF-source power were set as 550°C and 150 W respectively. The process gas pressure was kept at 10 mTorr using Ar and oxygen gas mixture whose oxygen content was controlled in detail in the range from ∼1.10 to ∼2.60% to prepare a set of VO_2 samples of different oxygen stoichiometry. For the systematic KFM, XPS, and transport property studies, three samples (thickness ∼200 nm) sputtered with oxygen content of ∼2.25, ∼1.25, and ∼1.10% were chosen and labeled as A, B, and C, respectively, henceforth.

2.2. X-ray Diffraction. The structural characteristics of three representative samples A−C were analyzed by X-ray diffraction (XRD) $2\theta-\omega$ scan (2θ is the angle between the incident and the diffracted X-ray beam; ω is the angle between the incident beam and the specimen surface). XRD was performed on a four-circle Bruker D8 Discover diffractometer equipped with a Cu X-ray tube, Göbel mirror, 4-bounce 022 Ge channel-cut monochromator (to select only the Cu $K_{\alpha 1}$ radiation), Eulerian cradle, and a scintillation counter.

2.3. Electrical Conductivity Measurement and X-ray Photoelectron Spectroscopy. The resistivity of VO_2 films was measured varying temperature on devices where VO_2 films are patterned by photolithography and Cr/Au electrodes are coated by thermal evaporation using four-probe methods in an environmental probe station equipped with a heating stage whose temperature is calibrated with thermocouples carefully. At each temperature, after thermal stabilization, a series of linear current-voltage ($I-V$) characteristic curves were recorded in galvanodynamic mode using Solartron electrochemical system (SI 1287) and the average resistance was calculated based on the linear fitting on the $I-V$ plots. In-depth XPS profiling was performed on SSX-100 ESCA XPS system using Al Kα x-ray source (1.4866 keV) and Ar ion sputtering in ultra-high vacuum condition (∼1 × 10^{-7} Torr). All XPS spectra were referenced to the C 1s peak.

2.4. Kelvin Force Microscopy. KFM was performed using Pt-coated conducting tips (MikroMasch DPER14) on Asylum MFP-3D Coax AFM system including a heating stage module in the temperature range from 300 to 368 K in the ambient environment. As a control for our measurement reported in this article, a Si-based reference structure was tested and the accuracy of Φ was estimated as ∼0.02 eV.[11] 30 nm-thick Au/Cr layer including windows of 2 × 0.2 mm^2 was coated on VO_2 films and used as grounded reference for Φ calibration. The samples were cleaned with acetone (ultrasonic) and isopropyl alcohol prior to measurements. To estimate Φ of VO_2, CPD was scanned across the interface between the reference Au surface and the uncoated VO_2 film region. Evaporated gold is commonly used as a reference in Kelvin force microscopy.[10−17] The scan region has a rectangular shape of 24 × 1.5 μm^2 size for full saturation of CPD in both sides. The tip height from the surface was maintained to be 15 nm. At each temperature, KFM scans were conducted continuously for at least 4−5 h until the thermal drift is eliminated and surface potential is stabilized.

3. RESULTS AND DISCUSSION

3.1. Structure. As shown in Figure 1, XRD $2\theta-\omega$ scan profiles were measured on samples A-C at room temperature. Samples A and B were characterized by XRD on as-grown films, whereas the XRD scans on sample C was conducted after device fabrication for electrical conductivity measurement and KFM experiments. Only XRD peaks corresponding to reflection

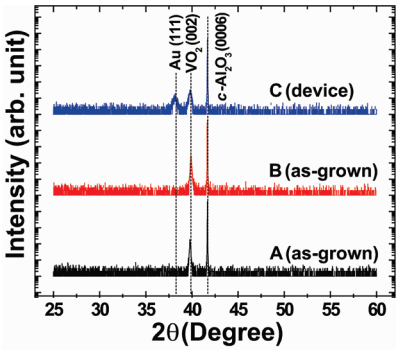

Figure 1. X-ray diffraction (XRD) $2\theta-\omega$ scan results obtained from samples A-C prepared with oxygen content of ∼2.25, ∼1.25, and ∼1.10%, respectively. Samples A and B was measured before fabrication process while Sample C was scanned in the device form including the electrode.

from (002) of monoclinic VO_2 phase were observed in addition to the substrate peaks (and Au peak only from sample C including metal electrode). These results indicate that the major phase of all films is highly textured VO_2 grown along the (0001) direction normal to the substrate.

3.2. Electrical Characterizations. The resistivity vs. temperature plots measured from the samples A−C are summarized in Figure 2a with an inset including the schematic image of the patterned device for electrical transport characterization by four terminal measurements. By measuring resistivity as a function of temperature spanning the transition regime, the MIT characteristics of bulk region of VO_2 films can be investigated. The edges of VO_2 films patterned by reactive ion etching are sharp as shown in AFM image in Figure 2b, and hence the measured resistivity is primarily determined by contribution from bulk of the film as displayed in Figure 2c. Sample A shows a sharp transition with the largest resistivity ratio of four orders via transition to metallic phase indicating that the average nominal film stoichiometry is closest to that of VO_2. On the other hand, the transition in sample B is relatively less sharp and with a lower transition temperature indicating that sample B includes more portion of phases of lower oxidation states as compared with sample A.[4] Sample C is observed to have only metallic characteristic in the whole temperature range without evident transition. Despite the similarity in XRD profiles of the samples, this trend is to be expected considering that sample A was grown with optimal gas configuration and others were prepared in more reduced environment intentionally and the MIT characteristic of the film is affected by the portion of non-VO_2 phases.[4]

3.3. Kelvin Force Microscopy Experiments. Each line scan of KFM mode is composed of a topography scan and a subsequent CPD measurement as shown schematically in Figure 3. The measured CPDs on Au (left) and VO_2 (right) sides are equal to $(\Phi_{tip} - \Phi_{Au})/e$ and $(\Phi_{tip}-\Phi_{VO2})/e$ respectively. Φ_{tip}, Φ_{Au}, and Φ_{VO2} indicate the work function of the surface of AFM tip, Au, and VO_2 each. Therefore, the Φ difference between Au and VO_2, $\Phi_{Au} - \Phi_{VO2}$, can be converted from CPD between Au and VO_2.

Figure 4 shows a surface topography map (a) and a series of CPD images (b−e) obtained by scanning the same area of sample A varying temperature along with the corresponding histograms to each CPD map (f). The topography map was flattened by first-order polynomial and the CPD scan images were rescaled setting the positions of the all histogram peaks

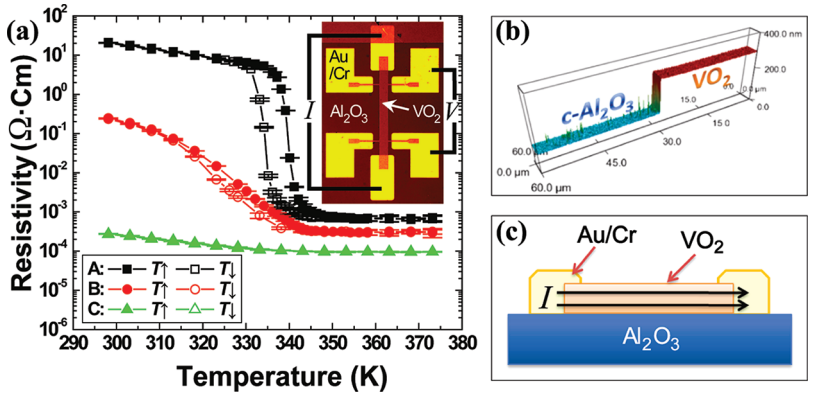

Figure 2. Summary of electrical measurements on VO_2 films with schematics. (a) Resistivity vs. temperature plots measured from samples A-C grown with oxygen content of ~2.25, ~1.25, and ~1.10%, respectively, with error bars of standard deviation from a series of conductivity measurements. The inset displays the image of device used for the four probe conductivity measurement (device width, ~200 μm; length, ~1200 μm). (b) Three-dimensional topographical image obtained by atomic force microscopy scanning across the edge of patterned VO_2 film prior to Au/Cr contact fabrication. (c) Schematic diagram of the patterned sample used for electrical transport measurements.

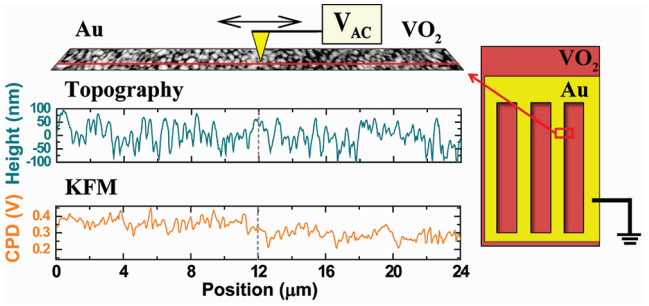

Figure 3. Schematic of Kelvin force microscopy.

corresponding to CPD on Au region same as that at 300 K because of the slight fluctuation of surface potential. From the distance of two peak positions in the histogram (i.e., CPD between Au and VO_2) determined by fitting with two overlapped Gaussian peaks, we can extract Φ_{VO2} using the reported Φ_{Au} value of 5.10 eV.[9,18,19] The Φ_{VO2} of sample A surface is almost constant ~5.17 to ~5.19 eV regardless of temperature though the sharp transition was verified in terms of resistivity representing film bulk properties. This result represents that the phase transition does not necessarily occur in the surface region of sample A because of the existence of more oxidized phase. This will be discussed further later. The contrast of KFM resembling grain structures is likely due to the existence of different stoichiometric phases along grain boundaries rather than the topographical effect as also observed by conductive AFM (C-AFM).[20]

On the other hand, as displayed in Figure 5b to 5e, slightly oxygen-deficient sample B shows an evident change in Φ_{VO2} as temperature increases. This can be seen clearly in the set of histograms displayed at varying temperature in Figure 5f. The Φ_{VO2} of sample B is observed to increase by ~0.15 eV via MIT under heating representing the major phase near the surface is VO_2. In the case of sample C (KFM images not shown), the increase of Φ is smaller as ~0.08 eV over the same temperature range indicating the fraction of VO_2 phase on sample C surface is relative lower than that on sample B surface. Though sample A shows better MIT properties of the bulk film, in terms of both morphology and surface MIT functionality, sample B could be more interesting for VO_2-based devices such as a field-effect transistor where primarily the properties of narrow channel region beneath surface are critical for device performance. The band structure of both monoclinic and rutile VO_2 phases has been explored by photoemission studies[21−23] as well as theoretical calculations.[24,25] Accordingly, the change of Φ driven by MIT is discussed using energy band diagram.[21,26,27] The Φ of metallic rutile VO_2 phase, Φ_M, equals to the ionization energy of metal phase, E_M, while Φ of insulating monoclinic VO_2 phase, Φ_I, is expressed by $\Phi_I = E_I + \Delta E_c$ where E_I is the ionization energy of insulator phase and ΔE_c is the energy difference between the bottom of conduction band and E_F. In a recent photoemission spectroscopy study on VO_2 thin films, ΔE_c was estimated to be ~0.1 eV or lower probably due to the existence of donor-like oxygen defects.[23] Therefore, using our results on sample B, the increase in ionization energy by the transition to metallic phase is estimated to be in the $E_M - E_I \approx 0.15-0.25$ eV range.

In Figure 6, Φ vs. temperature plots obtained from all samples are summarized. The inset shows the average Φ values at 300 K (square) and 368 K (circle) with error bars of standard deviation, which are calculated from a series of KFM measurements under repetitive heating cycles on different regions of devices. The small errors in Φ measurements indicate our KFM results are reproducible. By comparison with resistivity data in Figure 2a characterizing bulk film properties, we can clearly see the gap between MIT characteristics of surface and bulk-region of VO_2 films and such differences in surface and bulk transition characteristics in VO_2 has also been observed by scanning tunneling microscopy studies.[28] The gradual transition of Φ unlike the sharp jump of conductivity is likely caused by nonuniform stoichiometry near the film surface. There is then the question of how to reconcile this data with a recent UPS measurement of VO_2 nanostructures that the authors were made aware of during the review process.[8] It is well known that the phase transition and electronic structure of vanadium oxide is very sensitive to synthesis conditions and post-deposition processing.[4,16,29−33] It is hence possible that the samples being studied in the two works have subtle differences in surface composition or structure leading to this trend. Another possibility is the KFM experiment is performed in ambient and perhaps there is some dependence on humidity. These are speculations and further work is necessary to resolve the differences.

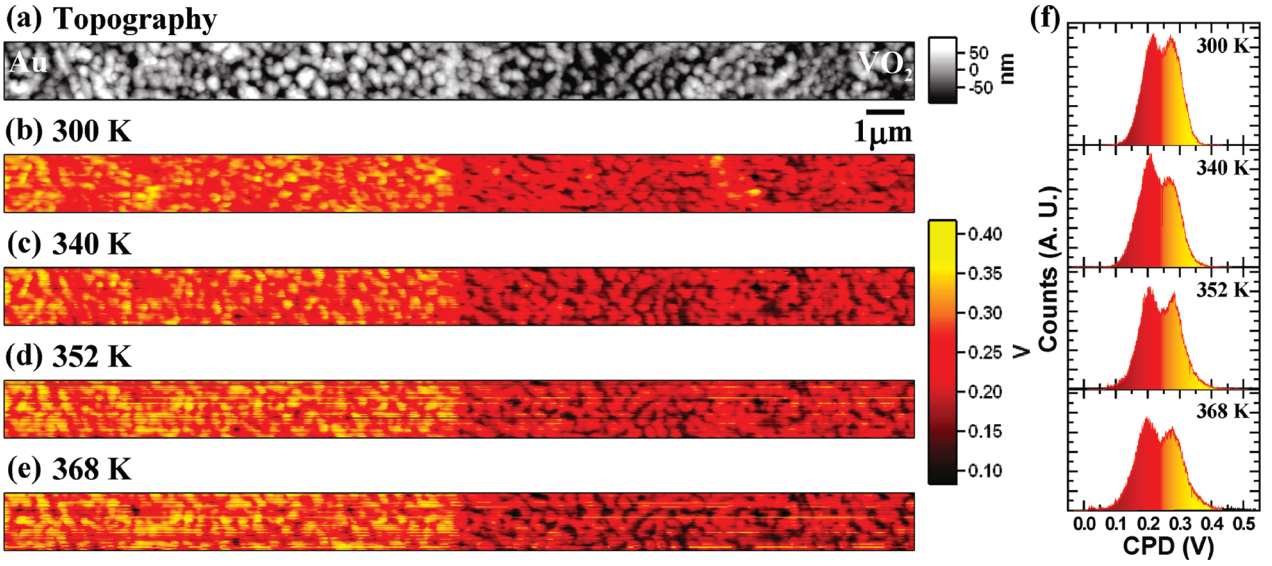

Figure 4. (a) First-order flattened surface topography map and (b-e) contact potential difference (CPD) scan images at varying temperatures measured on the identical region of sample A with (f) a set of histograms extracted from corresponding CPD maps in (b-e) respectively. The left half of scanned area is coated with ~30 nm thick Au/Cr layer on the VO_2 film for work function reference.

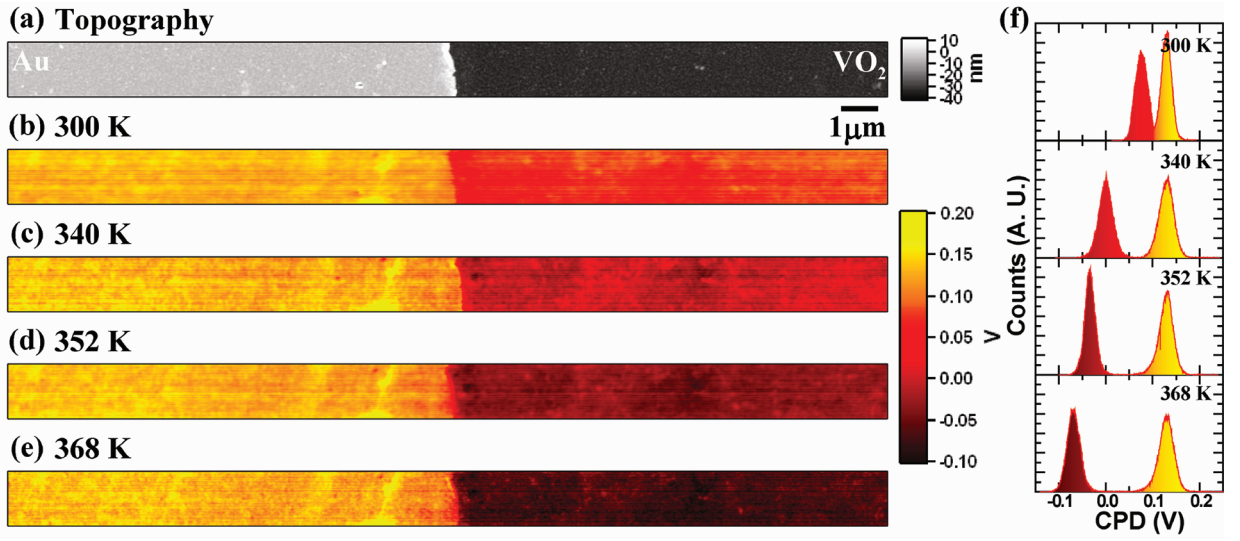

Figure 5. (a) First-order flattened surface topography map and (b−e) contact potential difference (CPD) scan images at varying temperatures measured on the identical region of sample B, with (f) a set of histograms extracted from corresponding CPD maps in (b−e), respectively. The left half of scanned area is coated with ~30 nm-thick Au/Cr layer on the VO_2 film for work function reference.

3.4. Depth-Dependent X-ray Photoelectron Spectroscopy. To understand the differences between surface and bulk MIT properties, we conducted XPS-based compositional characterization on the samples as a function of depth. Figure 7a shows three representative XPS spectra from sample C measured at the as-grown film surface and 35 and 70 nm depth from the surface respectively. Figure 7b includes an example of XPS-based composition analysis using XPS spectra corresponding to O 1s and V 2p peaks (of sample C). The ratio of O counts to V counts, denoted as $[O]_{count}$ and $[V]_{count}$ each, was calculated with the integrated area of O 1s and V $2p_{3/2}$ peaks given by Marquardt algorithm-based fitting with Shirley background using CasaXPS software and the XPS sensitivity factors, 2.46 and 5.42, for O 1s and V $2p_{3/2}$ peaks, respectively.[34] As summarized in Figure 7c, the stoichiometry for the samples is observed to vary as a function of depth consistent with literature reports.[35,36] At the surface, regardless of deposition conditions, the $[O]_{count}/[V]_{count}$ ratio is close to 2.5 (V_2O_5 phase) and decreases to ~1.8 with different decay rates depending on deposition conditions. Sample A grown with the highest oxygen content shows the slowest decrease rate in the $[O]_{count}/[V]_{count}$ ratio as a function of depth verifying the greater amount of VO_2 phase is present in sample A bulk than in the other samples. The off-stoichiometry in sample C verifies the poor MIT properties as observed in resistivity measurements. To consider the chemical state affecting the surface phase transition feature, the $[O]_{count}/[V]_{count}$ averaged over the screening length of VO_2

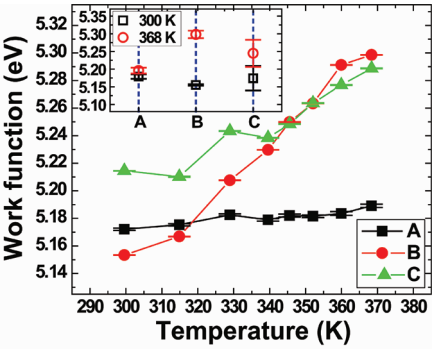

Figure 6. Work function vs. temperature plots measured from the surface of samples A-C with error bars from fitting process. The inset shows the average work function values with error bars representing standard deviation measured at 300 and 368 K under repeated heating cycles on different scanned regions.

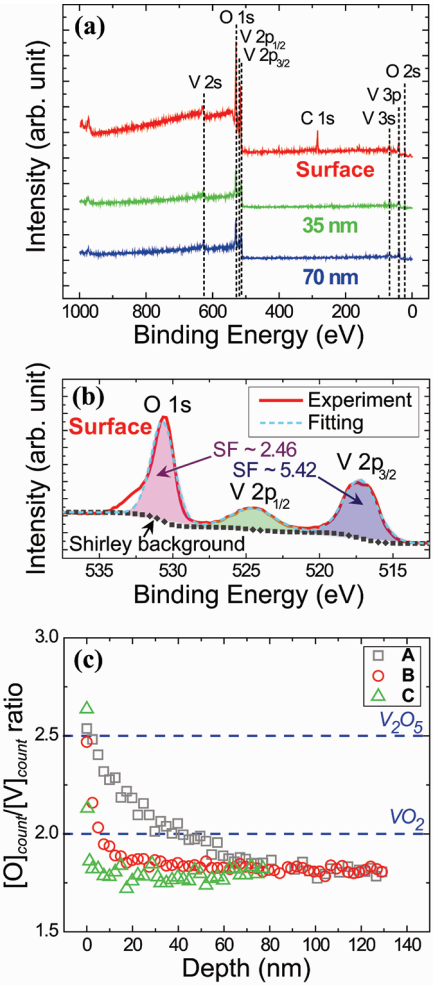

Figure 7. (a) Representative X-ray photoelectron spectroscopy (XPS) profiles measured at the VO_2 film surface and 35 nm and 70 nm depth from the surface of sample C. (b) High-resolution XPS spectrum of the sample C surface fitted for elemental composition analysis. SF stands for sensitivity factor. (c) The variation of the ratio of O counts, $[O]_{count}$, to V counts, $[V]_{count}$, of samples A-C as a function of the depth from VO_2 film surface estimated by XPS. Two dashed lines indicate the O/V composition ratio of V_2O_5 (2.5) and VO_2 (2) phases, respectively.

(~5 nm)[27] is estimated by the first order exponential decay fitting and the calculated average $[O]_{count}/[V]_{count}$ ratios of near-surface regions in samples A-C are ~2.4, ~2.2, and ~1.8, respectively. While the near-surface stoichiometry of sample A is close to that of V_2O_5 phase that does not undergo a MIT, $[O]_{count}/[V]_{count}$ ratios of the other samples are close to 2 (VO_2 phase).

4. CONCLUSIONS

Temperature-dependence of work function has been measured in vanadium dioxide thin film surfaces by Kelvin force microscopy. By comparing work function and electrical conductivity coupled with X-ray photoelectron spectroscopy studies, the importance of surface stoichiometry is elucidated.

AUTHOR INFORMATION

Corresponding Author
*E-mail: cko@fas.harvard.edu.

ACKNOWLEDGMENT

We acknowledge AFOSR Grant FA9550-08-1-0203and ONR Grant N00014-10-1-0131 for financial support. Device fabrication and KFM measurement were performed mainly at the Harvard University Center for Nanoscale Systems (CNS), a member of the National Nanotechnology Infrastructure Network (NNIN). We thank Yanjie Cui and Gulgun Aydogdu-Kuru for assistance with the X-ray diffraction experiments and Rafael Jaramillo for technical discussions regarding KFM experiments.

REFERENCES

(1) Imada, M.; Fujimori, A.; Tokura, Y. *Rev. Mod. Phys.* **1998**, *70*, 1039.
(2) Mott, N. F. *Rev. Mod. Phys.* **1968**, *40*, 677.
(3) Goodenough, J. B. *J. Solid State Chem.* **1971**, *3*, 490.
(4) Griffiths, C. H.; Eastwood, H. K. *J. Appl. Phys.* **1974**, *45*, 2201.
(5) Neaman, D. A. *Semiconductor Physics and Devices*, 3rd ed.; McGraw-Hill Publishing Ltd: New York, 2007.
(6) Kim, T.-H.; Angst, M.; Hu, B.; Jin, R.; Zhang, X.-G.; Wendelken, J. F.; Plummer, E. W.; Li, A.-P. *Proc. Nat. Acad. Sci. U.S.A.* **2010**, *107*, 5272.
(7) Wang, Y.; Zhang, Z. *Physica E* **2009**, *41*, 548.
(8) Yin, H.; Luo, M.; Yu, K.; Gao, Y.; Huang, R.; Zhang, Z.; Zeng, M.; Cao, C.; Zhu, Z. *ACS Appl. Mater. Interfaces* **2011**, *3*, 2057.
(9) Michaelson, H. B. *J. Appl. Phys.* **1977**, *48*, 4729.
(10) Nonnenmacher, M.; O'Boyle, M.; Wickramasinghe, H. K. *Ultramicroscopy* **1992**, *42-44*, 268.
(11) Jaramillo, R.; Ramanathan, S. *Sol. Energy Mater. Solar Cells* **2011**, *95*, 602.
(12) Nonnenmacher, M.; Oboyle, M. P.; Wickramasinghe, H. K. *Applied Physics Letters* **1991**, *58*, 2921.
(13) Takahashi, T.; Kawamukai, T. *Ultramicroscopy* **2000**, *82*, 63.
(14) McMurray, H. N.; Williams, G. *J. Appl. Phys.* **2002**, *91*, 1673.
(15) Shiraishi, M.; Shibata, K.; Maruyama, R.; Ata, M. *Phys. Rev. B* **2003**, *68*, 235414.
(16) Tomida, Y.; Nitta, S.; Kamiyama, S.; Amano, H.; Akasaki, I.; Otani, S.; Kinoshita, H.; Liu, R.; Bell, A.; Ponce, F. A. *Appl. Surf. Sci.* **2003**, *216*, 502.
(17) Shiraishi, M.; Takebe, K.; Matsuoka, K.; Saito, K.; Toda, N.; Kataura, H. *J. Appl. Phys.* **2007**, *101*, 014311.
(18) Schmitz, A.; Ping, A.; Khan, M.; Chen, Q.; Yang, J.; Adesida, I. *J. Elect. Mater.* **1998**, *27*, 255.
(19) Barbet, S.; Aubry, R.; Forte-Poisson, M.-A. d.; Jacquet, J.-C.; Deresmes, D.; Melin, T.; Theron, D. *Appl. Phys. Lett.* **2008**, *93*, 212107.

(20) Kim, J.; Ko, C.; Frenzel, A.; Ramanathan, S.; Hoffman, J. E. *Appl. Phys. Lett.* **2010**, *96*, 213106.
(21) Shin, S.; Suga, S.; Taniguchi, M.; Fujisawa, M.; Kanzaki, H.; Fujimori, A.; Daimon, H.; Ueda, Y.; Kosuge, K.; Kachi, S. *Phys. Rev. B* **1990**, *41*, 4993.
(22) Okazaki, K.; Wadati, H.; Fujimori, A.; Onoda, M.; Muraoka, Y.; Hiroi, Z. *Phys. Rev. B* **2004**, *69*, 165104.
(23) Ruzmetov, D.; Zawilski, K. T.; Senanayake, S. D.; Narayanamurti, V.; Ramanathan, S. *J. Phys.* **2008**, *20*, 465204.
(24) Wentzcovitch, R. M.; Schulz, W. W.; Allen, P. B. *Phys. Rev. Lett.* **1994**, *72*, 3389.
(25) Gatti, M.; Bruneval, F.; Olevano, V.; Reining, L. *Phys. Rev. Lett.* **2007**, *99*, 266402.
(26) Qazilbash, M. M.; Burch, K. S.; Whisler, D.; Shrekenhamer, D.; Chae, B. G.; Kim, H. T.; Basov, D. N. *Phys. Rev. B* **2006**, *74*, 205118.
(27) Ruzmetov, D.; Gopalakrishnan, G.; Ko, C.; Narayanamurti, V.; Ramanathan, S. *J. Appl. Phys.* **2010**, *107*, 114516.
(28) Yin, W.; Wolf, S.; Ko, C.; Ramanathan, S.; Reinke, P. *J. Appl. Phys.* **2011**, *109*, 024311.
(29) Fiermans, L.; Vennik, J. *Surf. Sci.* **1971**, *24*, 541.
(30) grymonprez, G.; Fiermans, L.; Vennik, J. *Surf. Sci.* **1973**, *36*, 370.
(31) Toledano, D. S.; Metcalf, P.; Henrich, V. E. *Surf. Sci.* **2001**, *472*, 21.
(32) Sahana, M. B.; Subbanna, G. N.; Shivashankar, S. A. *J. Appl. Phys.* **2002**, *92*, 6495.
(33) Ruzmetov, D.; Senanayake, S. D.; Ramanathan, S. *Phys. Rev. B* **2007**, *75*, 195102.
(34) http://www.npl.co.uk/nanoscience/surface-nanoanalysis/products-and-services/xps-and-aes-average-matrix-relative-sensitivity-factors.
(35) Ghanashyam Krishna, M.; Debauge, Y.; Bhattacharya, A. K. *Thin Solid Films* **1998**, *312*, 116.
(36) Lu, S.; Hou, L.; Gan, F. *Thin Solid Films* **1999**, *353*, 40.